Research Article

Land surface temperature and normalized difference vegetation index relationship: a seasonal study on a tropical city

Subhanil Guha[1] · Himanshu Govil[1]

Received: 7 April 2020 / Accepted: 27 August 2020 / Published online: 9 September 2020
© Springer Nature Switzerland AG 2020

Abstract
Land surface temperature (LST) and its relationship with normalized difference vegetation index (NDVI) are significantly considered in environmental study. The aim of this study was to retrieve the LST of Raipur City of tropical India and to explore its seasonal relationships with NDVI. Landsat images of four specific seasons for three particular years with fourteen years time interval were analyzed. The result showed a gradual rising (3.63 °C during 1991–2004 and 1.54 °C during 2004–2018) of LST during the whole period of study. The mean LST value of three particular years was the lowest (27.21 °C) on green vegetation and the highest (29.81 °C) on bare land and built-up areas. The spatial distribution of NDVI and LST reflects an inverse relationship. The best (− 0.63) and the least (− 0.17) correlation were noticed in the post-monsoon and winter seasons, respectively, whereas a moderate (− 0.45) correlation were found both in the monsoon and pre-monsoon seasons. This LST-NDVI correlation was strong negative (− 0.51) on vegetation surface, moderate positive on water bodies (0.45), and weak positive on the built-up area and bare land (0.14). In summary, the LST is greatly controlled by surface characteristics. This study can be used as a reference for land use and environmental planning in a tropical city.

Keywords Landsat · LST · NDVI · Tropical city

1 Introduction

Urbanization accelerates the ecological stress by warming the local or global cities for a large extent [1–6]. Presently, many urban areas are suffering with a huge land conversion and resultant new heat zones [7–9]. Remote sensing techniques are significantly effective in detecting the land use/land cover (LULC) change and its consequences [10]. Several satellite sensors are capable to identify these change zones by using their visible and near-infrared (VNIR) and shortwave infrared (SWIR) bands [11]. Apart from the conventional LULC classification algorithms, some spectral indices are used in detecting specific land features. Normalized difference vegetation index (NDVI) can be considered as the most applied spectral index in this scenario [12]. Recently, thermal infrared (TIR) bands are also used by generating some indices for different types of LULC extraction [13–15]. These remote sensing indices are used significantly in several application fields like rocks and mineral mapping, forest mapping, agricultural monitoring, LULC mapping, hazard mapping, urban heat island mapping and monitoring, among others [14, 16–19].

Land surface temperature (LST) retrieved from several remotely sensed data is widely used in the detection of urban heat island and ecological comfort zone [20–23]. LST can change significantly in a vast homogeneous land surface or even inside a relatively small heterogeneous urban area [14, 24, 25]. Different types of LULC response differently in TIR band and consequently LST largely varies in an urban environment [26–44]. The LULC types are mainly changed by land conversion process [10]. Thus, time is an important factor in LST monitoring. These spatial and temporal data of LST is also varied with the

✉ Subhanil Guha, subhanilguha@gmail.com | [1]Department of Applied Geology, National Institute of Technology, Raipur, India.

seasonal changes as sun elevation and sun azimuth are changed with seasons. Hence, the seasonal variation of LST is quite important in any LULC related study.

NDVI is a dominant factor in LST derivation processes and is used invariably in any LST related study [45–49]. NDVI is directly used in the determination of land surface emissivity and thus is a significant factor for LST estimation [50, 51]. It also determines the LULC categories by its optimum threshold limits in different physical environment [14]. Being a vegetation index, NDVI depends largely on seasonal variation [12]. Hence, LST is also regulated by the change of seasons. Thus, seasonal evaluation of LST and NDVI is an important task in LST mapping and monitoring, especially in an urban landscape.

The relationship of LST with NDVI is quite interesting and it attracts the remote sensing scientists from several directions [52–55]. The nature and strength of this relationship heavily depend on space and time. Generally, in the tropical environment the LST-NDVI relationship is negative [56–58]. The negativity of the relationship is determined by the changing type of LULC over time. Thus, spatial and temporal changes in this relationship are observed on different types of LULC. Apart from the spatial and temporal changes, seasonal variation of LST-NDVI relationship is a very important study in any mixed urban land surface.

Several studies are available on the seasonal analysis of LST-NDVI relationship. Many tropical cities are a part of these studies. Many valuable research articles found on LST-NDVI relationships in the Chinese landscape [59–67]. Some studies were also performed in Indian urban landscape [35, 36, 68–71].These studies found that LST builds a negative relationship with NDVI and this negativity can change with season. Wet season reflects a stronger negative correlation than dry season as the moisture content is more in the wet season [72]. This relationship can also change with the change of land surface types. Vegetation surface builds a strong correlation and the strength is reduced on bare land surface, built-up surface, and water surface.

The present study calculates the LST and NDVI from Landsat datasets of four different seasons (winter, pre-monsoon, monsoon, and post-monsoon) in Raipur City of India using a total of 12 Landsat satellite images for 1991, 2004, and 2018. Meanwhile, the LULC map has been obtained by suitable threshold values of NDVI. The main aims of the study were (1) to analyze the seasonal variation of spatial distribution pattern of the LST in the study area, (2) to determine the seasonal variation of LST-NDVI relationship for whole of the city, and (3) to explore the seasonal variation of LST-NDVI relationship on different LULC types.

2 Study area and data

Figure 1 shows the study area (Raipur City of India) of the present research work including the false colour composite (FCC) image of and digital elevation model (DEM) image. Raipur is one of the fastest-growing smart cities in India. The latitudinal and longitudinal extent of the city is from 21°11′22″ N to 21°20′02″ N and from 81°32′20″ E to 81°41′50″ E. The total area of the city is approximately 164.23 km^2. The only big river is Mahanadi which flows along the eastern boundary of Raipur. The southern part of the city is covered by dense forests. Geologically the city is very stable. According to India Meteorological Department (IMD) (https://mausam.imd.gov.in) [75], the study area is under a tropical wet and dry climate with four typical seasons (pre-monsoon, monsoon, post-monsoon, and winter). May is the hottest month followed by April, June, and March. July is the rainiest month followed by August, June, and September. October and November are the post-monsoon months experience a pleasant weather condition. December (the coldest month), January, and February are the winter months. The pre-monsoon and winter months (including November) remain dry compared to the monsoon and post-monsoon months.

Four Landsat 8 Operational Land Imager (OLI) and Thermal Infrared Sensors (TIRS) data of 2018; four Landsat 5 Thematic Mapper (TM) data of 2004; and four Landsat 5 TM data of 1991 have been freely downloaded from the United States Geological Survey (USGS) (https://earthexplorer.usgs.gov) Data Centre (Table 1). Landsat 8 TIRS dataset has two TIR bands (bands 10 and 11) in which band 11 has uncertainty in calibration. Thus, only TIR band 10 (100 m resolution) has been recommended for the present study. The TIR band 10 has been resampled to 30 m × 30 m pixel size with cubic convolution method by the USGS. Landsat 5 TM data has only one TIR band (band 6) of 120 m resolution which has also been resampled to 30 m × 30 m pixel size with cubic convolution method by the USGS. The spatial resolution of visible to near infrared (VNIR) bands of the two types of Landsat datasets is 30 m.

3 Methodology

3.1 Retrieving LST from Landsat data

In this study, the mono-window algorithm was applied to retrieve LST from multi-temporal Landsat satellite sensors [1, 76–79] where three necessary parameters are ground emissivity, atmospheric transmittance, and effective mean atmospheric temperature. At first, the original TIR bands (100 m resolution for Landsat 8 OLI/TIRS data,

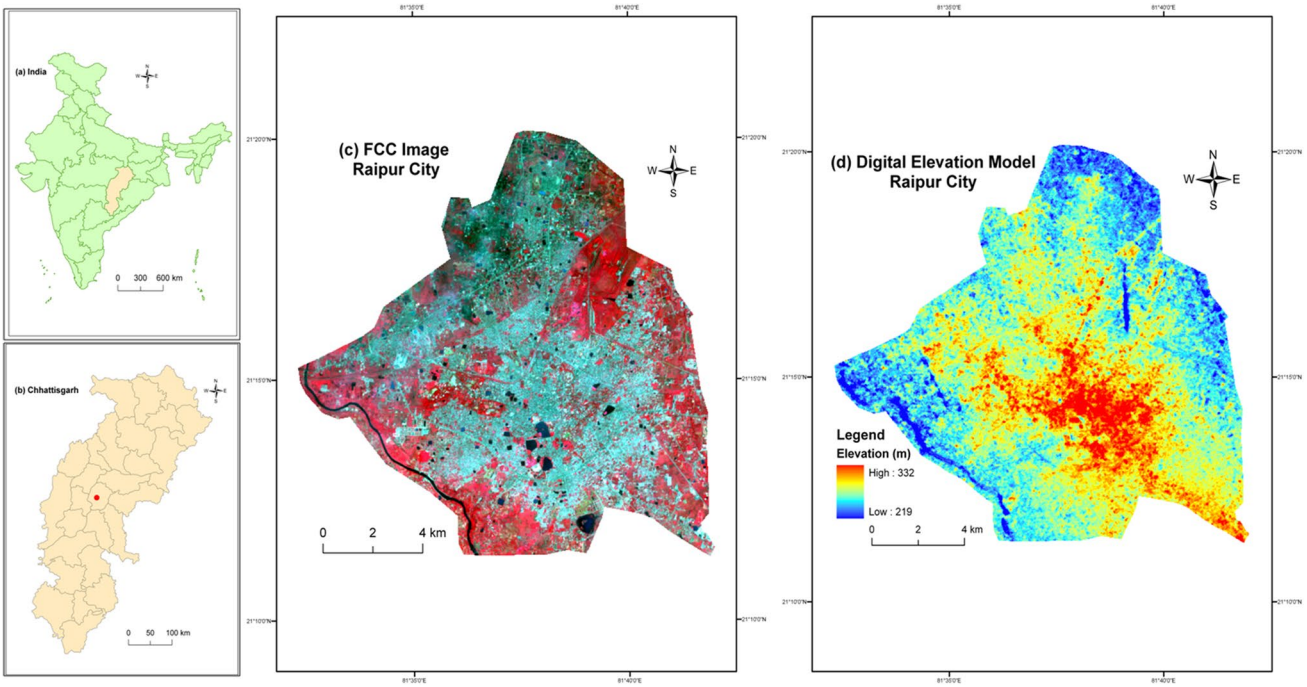

Fig. 1 Location of the study area: **a** India **b** Chhattisgarh **c** FCC image of Raipur City **d** DEM image of Raipur City (*Source*: https://earthexplorer.usgs.gov [73] and http://www.surveyofindia.gov.in [74])

Table 1 Specification of Landsat data sets (*Source*: USGS)

Season	Date of acquisition	Path-row	Resolution of VNIR bands (m)	Resolution of TIR bands (m)
Pre-monsoon	18-Mar-1991	142–045	30	120
	22-Apr-2004	142–045	30	120
	28-Mar-2018	142–045	30	100
Monsoon	26-Sep-1991	142–045	30	120
	09-Jun-2004	142–045	30	120
	16-Jun-2018	142–045	30	100
Post-monsoon	12-Oct-1991	142–045	30	120
	15-Oct-2004	142–045	30	120
	22-Oct-2018	142–045	30	100
Winter	14-Feb-1991	142–045	30	120
	02-Dec-2004	142–045	30	120
	08-Feb-2018	142–045	30	100

120 m resolution for Landsat 5 TM data) were resampled into 30 m by USGS data centre for further application.

The TIR pixel values are firstly converted into radiance from digital number (DN) values. Radiance for TIR band of Landsat 5 TM data is obtained using Eq. (1) (USGS):

$$L_\lambda = \left[\frac{L_{MAX\lambda} - L_{MIN\lambda}}{QCAL_{MAX} - QCAL_{MIN}}\right] * \left[Q_{CAL} - QCAL_{MIN}\right] + L_{MIN\lambda} \quad (1)$$

where L_λ is Top of Atmosphere (TOA) spectral radiance ($Wm^{-2}\ sr^{-1}\ mm^{-1}$), Q_{CAL} is the quantized calibrated pixel value in DN, $L_{MIN\lambda}$ ($Wm^{-2}\ sr^{-1}\ mm^{-1}$) is the spectral radiance scaled to $QCAL_{MIN}$, $L_{MAX\lambda}$ ($Wm^{-2}\ sr^{-1}\ mm^{-1}$) is the

spectral radiance scaled to $QCAL_{MAX}$, $QCAL_{MIN}$ is the minimum quantized calibrated pixel value in DN and $QCAL_{MAX}$ is the maximum quantized calibrated pixel value in DN. $L_{MIN\lambda}$, $L_{MAX\lambda}$, $QCAL_{MIN}$, and $QCAL_{MAX}$ values are obtained from the metadata file of Landsat TM data. Radiance for Landsat 8 TIR band is obtained from Eq. (2) [80]:

$$L_\lambda = M_L \cdot Q_{CAL} + A_L \tag{2}$$

where L_λ is the TOA spectral radiance ($Wm^{-2}\ sr^{-1}\ mm^{-1}$), M_L is the band-specific multiplicative rescaling factor from the metadata, A_L is the band-specific additive rescaling factor from the metadata, Q_{CAL} is the quantized and calibrated standard product pixel values (DN). All of these variables can be retrieved from the metadata file of Landsat 8 data.

For Landsat 5 data, the reflectance value is obtained from radiances using Eq. (3) (USGS):

$$\rho_\lambda = \frac{\pi \cdot L_\lambda \cdot d^2}{ESUN_\lambda \cdot \cos\theta_s} \tag{3}$$

where ρ_λ is unitless planetary reflectance, L_λ is the TOA spectral radiance ($Wm^{-2}\ sr^{-1}\ \mu m^{-1}$), d is Earth-Sun distance in astronomical units, $ESUN_\lambda$ is the mean solar exo-atmospheric spectral irradiances ($Wm^{-2}\ \mu m^{-1}$) and θ_s is the solar zenith angle in degrees. $ESUN_\lambda$ values for each band of Landsat 5 can be obtained from the handbooks of the related mission. θ_s and d values can be attained from the metadata file.

For Landsat 8 data, reflectance conversion can be applied to DN values directly as in Eq. (4) [80]:

$$\rho_\lambda = \frac{M_\rho \cdot Q_{CAL} + A_\rho}{\sin\theta_{SE}} \tag{4}$$

where M_ρ is the band-specific multiplicative rescaling factor from the metadata, A_ρ is the band-specific additive rescaling factor from the metadata, Q_{CAL} is the quantized and calibrated standard product pixel values (DN) and θ_{SE} is the local sun elevation angle from metadata file.

Equation (5) is used to convert the spectral radiance to at-sensor brightness temperature [81, 14]:

$$T_b = \frac{K_2}{\ln\left(\frac{K_1}{L_\lambda} + 1\right)} \tag{5}$$

where T_b is the brightness temperature in Kelvin (K), L_λ is the spectral radiance in $Wm^{-2}\ sr^{-1}\ mm^{-1}$; K_2 and K_1 are calibration constants. For Landsat 8 data, K_1 is 774.89, K_2 is 1321.08 ($Wm^{-2}\ sr^{-1}\ mm^{-1}$). For Landsat 5 data, K_1 is 607.76, K_2 is 1260.56 ($Wm^{-2}\ sr^{-1}\ mm^{-1}$).

The land surface emissivity ε, is estimated using the NDVI Thresholds Method [51, 82].

In NDVI Threshold Method, there are three following equations:

a. $NDVI < 0.2$ for bare soil;
b. $NDVI > 0.5$ for vegetation;
c. $0.2 <= NDVI <= 0.5$ for mixed land with bare soil and vegetation.

In the last case, ε is estimated from Eq. (6):

$$\varepsilon = \varepsilon_v F_v + \varepsilon_s(1 - F_v) + d\varepsilon \tag{6}$$

where ε is land surface emissivity, ε_v is vegetation emissivity, ε_s is soil emissivity, Fv is fractional vegetation, $d\varepsilon$ is the effect of the geometrical distribution of the natural surfaces and internal reflections that can be expressed by Eq. (7):

$$d\varepsilon = (1 - \varepsilon_s)(1 - F_v)F\varepsilon_v \tag{7}$$

where ε_v is vegetation emissivity, ε_s is soil emissivity, Fv is fractional vegetation, F is a shape factor whose mean is 0.55, the value of $d\varepsilon$ may be 2% for mixed land surfaces [51].

The fractional vegetation F_v, of each pixel, is determined from the NDVI using Eq. (8) [50]:

$$F_v = \left(\frac{NDVI - NDVI_{\min}}{NDVI_{\max} - NDVI_{\min}}\right)^2 \tag{8}$$

where $NDVI_{\min} = 0.2$ and $NDVI_{\max} = 0.5$.

Finally, the land surface emissivity ε can be expressed by Eq. (9):

$$\varepsilon = 0.004 * F_v + 0.986 \tag{9}$$

where ε is land surface emissivity, Fv is fractional vegetation.

Water vapour content is estimated by Eq. (10) [29, 83]:

$$w = 0.0981 * \left[10 * 0.6108 * \exp\left(\frac{17.27 * (T_0 - 273.15)}{237.3 + (T_0 - 273.15)}\right) * RH\right] + 0.1697 \tag{10}$$

where w is the water vapour content (g/cm^2), T_0 is the near-surface air temperature in Kelvin (K), RH is the relative humidity (%). These parameters of atmospheric profile are the average values of 14 stations around Raipur which are obtained from the Meteorological Centre, Raipur (http://www.imdraipur.gov.in) [84] and the Regional Meteorological Centre, Nagpur (http://www.imdnagpur.gov.in [85]). Atmospheric transmittance is determined for Raipur City using Eq. (11) [76, 86]:

$$\tau = 1.031412 - 0.11536w \tag{11}$$

where τ is the total atmospheric transmittance, ε is the land surface emissivity.

Raipur City is located in the tropical region. Thus, Eq. (12) is applied to compute the effective mean atmospheric transmittance of Raipur [76, 86]:

$$T_a = 17.9769 + 0.91715T_0 \quad (12)$$

LST is retrieved from Landsat 5 TM and Landsat 8 OLI/TIRS satellite data by using Eqs. (13–15) [76]:

$$T_s = \frac{\left[a(1-C-D)+(b(1-C-D)+C+D)T_b - DT_a\right]}{C} \quad (13)$$

$$C = \varepsilon\tau \quad (14)$$

$$D = (1-\tau)[1+(1-\varepsilon)\tau] \quad (15)$$

where ε is the land surface emissivity, τ is the total atmospheric transmittance, C and D are internal parameters based on atmospheric transmittance and land surface emissivity, T_b is the at-sensor brightness temperature, T_a is the mean atmospheric temperature, T_0 is the near-surface air temperature, T_s is the land surface temperature, $a = -67.355351, b = 0.458606$.

3.2 Extraction of different types of LULC by using the threshold limits of NDVI

NDVI can extract different types of LULC by using the optimum threshold values [14, 87–89]. This threshold values can differ with respect to the differences in physical environment. The NDVI threshold limits were applied on the post-monsoon images to extract the different LULC types accurately. Table 2 presents the suitable threshold limits of NDVI used for extracting the vegetation (> 0.2), water bodies (< 0), built-up area/bare land (0–0.2) in the study area.

4 Results and discussion

4.1 Accuracy assessment for LULC classification

The maximum likelihood classification method was applied to validate NDVI threshold based LULC classification. The overall accuracy values of the LULC classification were 95.00%, 85.00%, and 87.50% in 1991, 2004, and 2018, respectively. The kappa coefficients for the LULC classification were 0.91, 0.76, and 0.78 in 1991, 2004, and 2018, respectively. The kappa coefficient value of > 0.75 reflects the compatibility of the classification method [90]. In the present study, the average overall accuracy and average kappa coefficient were 89.17% and 0.82, respectively. Thus, the NDVI threshold method based LULC classification was significantly validated.

4.2 Extraction of LULC types using NDVI

Figure 2 shows the FCC images and LULC maps of the post-monsoon Landsat images of 1991, 2004, and 2018. Generally, the post-monsoon images reduce the level of air pollution due to the presence of high moisture content in the air and these images also enhance the greenness of an area. Thus, the post-monsoon images are generally considered for the generation of LULC maps. LULC maps were generated using the threshold limits of NDVI for different types of LULC by using ArcGIS software (https://www.esri.com/) [91]. In 1991, built-up area and bare land are mainly found in the northwest and middle portions of the city. Land conversion accelerates the decrease of vegetal covered area especially during 2004-2018. The major segment of vegetation is mainly found in the east and southwest parts of the city.

4.3 Characteristics of the spatial distribution of LST and NDVI

Table 3 shows the LST and NDVI values for different multi-date satellite data. The pre-monsoon image (Fig. 3) has the maximum values of mean LST (29.50 °C in 1991, 36.80 °C in 2004, and 37.90 °C in 2018) followed by monsoon (Fig. 4) image (25.74 °C in 1991, 29.23 °C in 2004, and 31.08 °C in 2018), post-monsoon (Fig. 5) image (24.99 °C in 1991, 27.56 °C in 2004, and 29.01 °C in 2018), and winter (Fig. 6) image (23.99 °C in 1991, 25.17 °C in 2004, and 26.91 °C in 2018). The mean LST of the city is increased by 8.40 °C in the pre-monsoon season, 5.34 °C in the monsoon season, 4.02 °C in the post-monsoon season, and 2.92 °C in the winter season during the whole time span (1991–2018). In the case of NDVI, the maximum value is decreased gradually with time (Figs. 3, 4, 5 and 6). Seasonally, the highest values of NDVI are observed in the post-monsoon images followed by the

Table 2 NDVI used for extracting different types of LULC [14]

Acronym	Description	Formulation	References	Threshold limits of NDVI for extracting different LULC types		
				Vegetation	Water bodies	Built-up area and bare land
NDVI	Normalized difference vegetation index	$\frac{NIR-Red}{NIR+Red}$	[87]	> 0.2	< 0	[0–0.2]

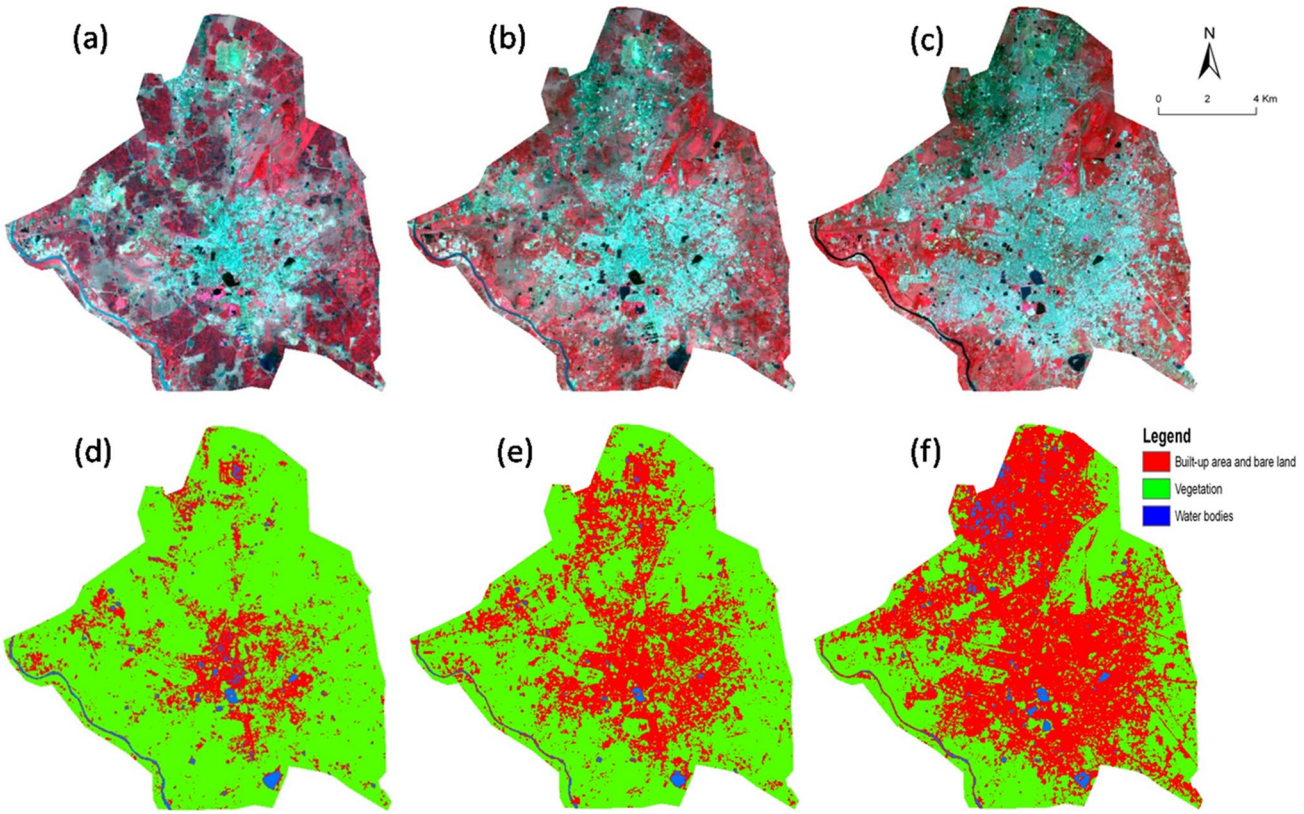

Fig. 2 FCC satellite images of post-monsoon season: **a** 14-OCT-1991 **b** 15-OCT-2004 **c** 22-OCT-2018; LULC maps in post-monsoon season: **d** 12-OCT-1991 **e** 15-OCT-2004 **f** 22-OCT-2018

Table 3 Temporal and seasonal variation of LST, NDVI, and LST-NDVI relationship (1991–2018)

Season	Date of acquisition	LST (°C)				NDVI				Correlation coefficient for LST-NDVI
		Min.	Max.	Mean	Std.	Min.	Max.	Mean	Std.	
Pre-monsoon	18-MAR-1991	22.81	34.46	29.50	1.27	−0.31	0.57	0.09	0.07	−0.40
	22-APR-2004	26.67	41.83	36.80	1.94	−0.32	0.59	0.07	0.08	−0.51
	28-MAR-2018	27.78	44.28	37.90	2.25	−0.16	0.50	0.10	0.06	−0.45
Monsoon	26-SEP-1991	22.38	30.83	25.74	1.41	−0.22	0.61	0.29	0.10	−0.48
	09-JUN-2004	22.81	33.26	29.23	1.58	−0.32	0.60	0.06	0.08	−0.41
	16-JUN-2018	25.49	34.98	31.08	1.13	−0.15	0.48	0.17	0.07	−0.47
Post-monsoon	12-OCT-1991	21.06	30.83	24.99	1.86	−0.27	0.64	0.32	0.11	−0.63
	15-OCT-2004	23.25	34.06	27.56	1.75	−0.41	0.70	0.31	0.15	−0.63
	22-OCT-2018	24.86	35.52	29.01	1.36	−0.14	0.48	0.18	0.08	−0.63
Winter	14-FEB-1991	14.71	30.01	23.99	2.21	−0.35	0.64	0.12	0.08	−0.12
	02-DEC-2004	19.73	31.64	25.17	1.34	−0.31	0.54	0.08	0.08	−0.20
	08-FEB-2018	21.99	32.53	26.91	1.30	−0.16	0.46	0.08	0.05	−0.18

monsoon, pre-monsoon, and winter images. The figures show that the proportion of vegetation is gradually reduced with time and NDVI is inversely related to LST.

4.4 Relationship between LST and LULC

The LST of the study area is significantly dependent upon the LULC types. Actually, this NDVI-threshold based emissivity method is not suitable for LST extraction of water

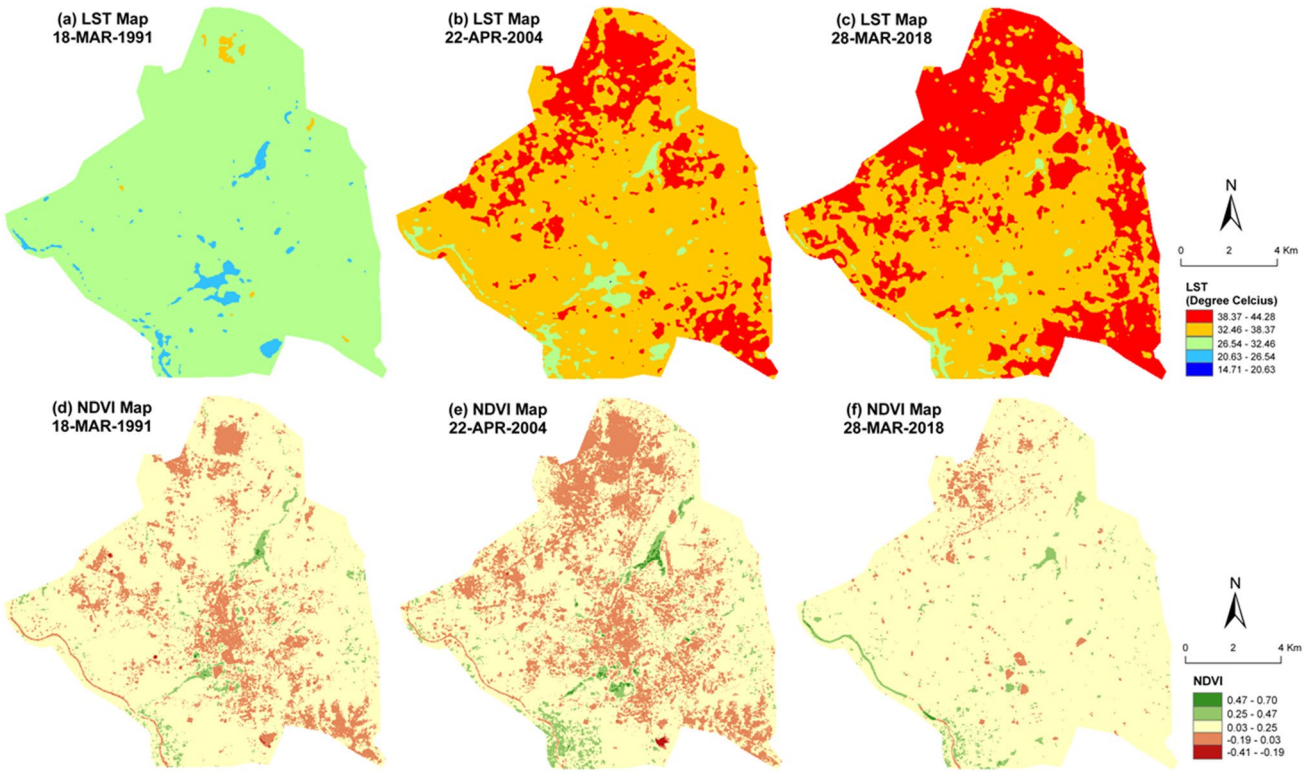

Fig. 3 Spatial distribution of LST in pre-monsoon season: **a** 18-MAR-1991 **b** 22-APR-2004 **c** 28-MAR-2018; spatial distribution of NDVI in pre-monsoon season: **d** 18-MAR-1991 **e** 22-APR-2004 **f** 28-MAR-2018

bodies. However, the present results show that the area with green vegetation has low LST value, whereas the built-up areas and bare lands have moderate to high LST value. In pre-monsoon season, built-up area and bare land has comparatively high LST than the other LULC types. But in the winter season, these areas have comparatively low to moderate LST due to low emissivity. The green areas and water areas are characterized by a relatively stable range of LST.

4.5 LST variation with the change in LULC types

Table 4 presents the temporal changes in LST with the changes in LULC types. Only the post-monsoon images of 1991, 2004, and 2018 were considered for this analysis. Generally, the land is converted into the built-up area or bare land from the other types of LULC, e.g., vegetation or water bodies. No such exceptional cases are seen in Raipur City during the entire period. Built-up area and bare land are increased while vegetation and water bodies are decreased significantly. The mean LST of the built-up area and bare land is increased from 1991 to 2004 (4.23 °C in post-monsoon season) and from 2004 to 2018 (1.49 °C in post-monsoon season), irrespective of any season. The green area gains 4.66 °C mean LST when it is converted into the built-up area and bare land between 1991 and 2018, and gained 2.20 °C mean LST between 2004 and 2018. The converted land from water bodies to the built-up area and bare land gains 2.49 °C during 1991–2018 and 0.96 °C mean LST during 2004–2018, respectively. Furthermore, the unchanged built-up area and bare land have also witnessed an increase in LST during the entire time span (2.79 °C mean LST from 1991 to 2018 and 0.83 °C mean LST from 2004 to 2018). Hence, the results indicate significantly to the trend of climate change.

4.6 Seasonal variation on LST-NDVI relationship

Table 3 presented the seasonal variation of mean LST values. Winter images indicate the lowest mean LST for 1991, 2004, and 2018. The highest mean LST values are found in the pre-monsoon images for all the three years. From 1991 to 2004, mean LST has been increased in every season. From 2004 to 2018, mean LST has been increased again for all the seasons. Post-monsoon images have mean LST value nearer to winter images while monsoon images have a slightly high value of mean LST than the post-monsoon images. Figure 7a–d show the seasonal variation of LST-NDVI relationships on different LULC types in pre-monsoon, monsoon, post-monsoon, and winter

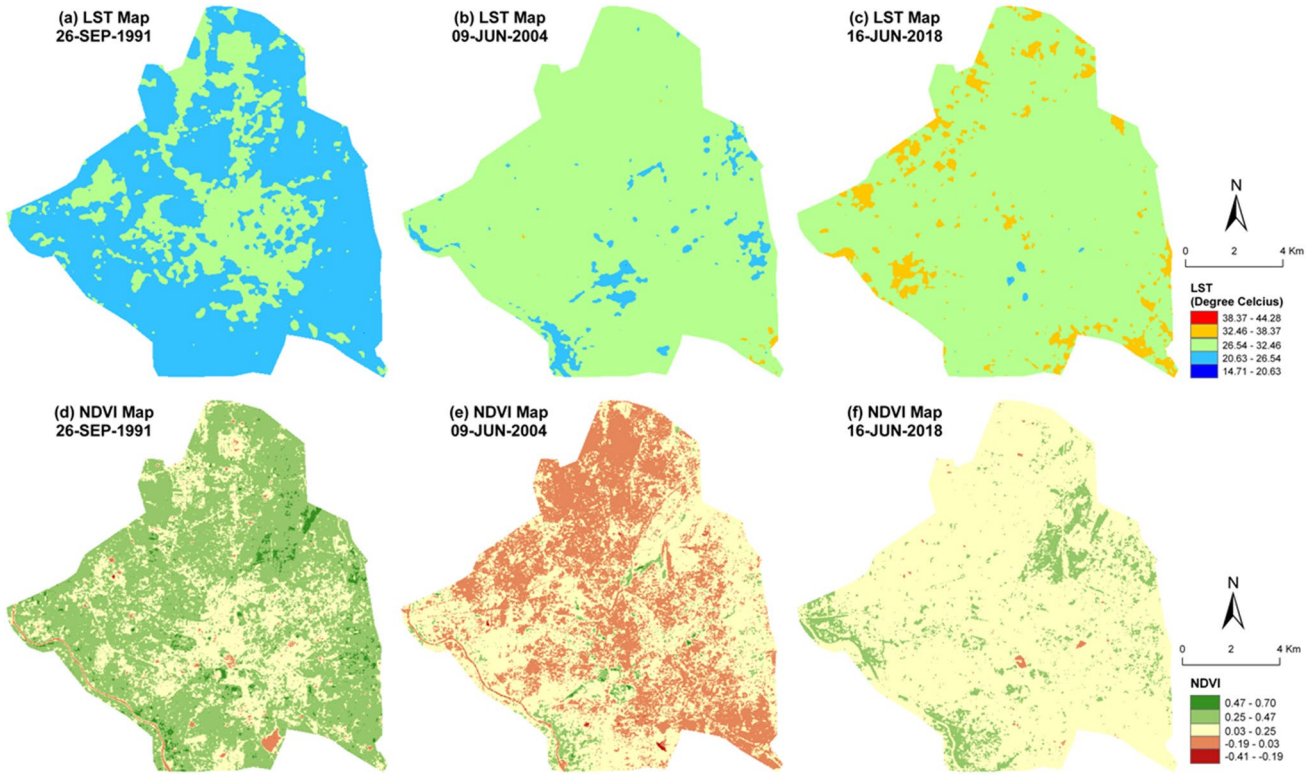

Fig. 4 Spatial distribution of LST in monsoon season: **a** 26-SEP-1991 **b** 09-JUN-2004 **c** 16-JUN-2018; spatial distribution of NDVI in monsoon season: **d** 26-SEP-1991 **e** 09-JUN-2004 **f** 16-JUN-2018

season, respectively. Here, only three types of LULC were considered, i.e., (1) vegetation, (2) water bodies, and (3) built-up area and bare land. On vegetation, the LST-NDVI relationships were negative, irrespective of any season. Only winter season (Fig. 7d) has weak negative regression, while the other three seasons (Fig. 7a–c) have moderate to strong negative regression. Since, NDVI is a vegetation index the LST-NDVI relationship is strongly effective on vegetation. On water bodies, the relationship is positive (weak to moderate). In the post-monsoon season (Fig. 7c), the relationship is weak to moderate. In the rest of the three seasons (Fig. 7a–d), the relationship is moderate. On the built-up area and bare land, the relationship is not so much significant. All four seasons (Fig. 7a–d) indicate weak regression as the surface materials become more heterogeneous in nature. Figure 7e represents a generalized view of the overall seasonal variation of LST-NDVI relationships. The relationship is negative, irrespective of any season. In winter, the relationship was weak negative (−0.12 in 1991, −0.2 in 2004, and −0.20 in 2018). The pre-monsoon and monsoon season built a moderately negative LST-NDVI relationship. In the pre-monsoon season, the correlation coefficient values of LST-NDVI relationship were −0.40 (1991), −0.51 (2004), and −0.45 (2018). In post-monsoon season, these correlation coefficient values were −0.48 in 1991, −0.41 in 2004, and −0.47 in 2018. The post-monsoon season built a stable and strong negative correlation. The correlation coefficient values of LST-NDVI relationship were −0.63 for all the 3 years. Hence, the post-monsoon season reveals the best correlation among the four seasons. It was mainly due to the high intensity of moisture and chlorophyll content in green vegetation. Dry atmosphere reduces the strength of correlation, whereas the wet seasons (post-monsoon and monsoon) enhance the strength of correlation.

Liang et al. [92], Ghobadi et al. [27], and Guha et al. [24] observed a negative LST-NDVI relationship in their study. A significant positive linear LST-NDVI relationship was observed between LST and NDVI [93]. In Shanghai City, Yue et al. [56] showed a negative LST-NDVI relationship and it varied on different LULC types. Sun and Kafatos [94] stated that LST-NDVI correlation was positive in winter

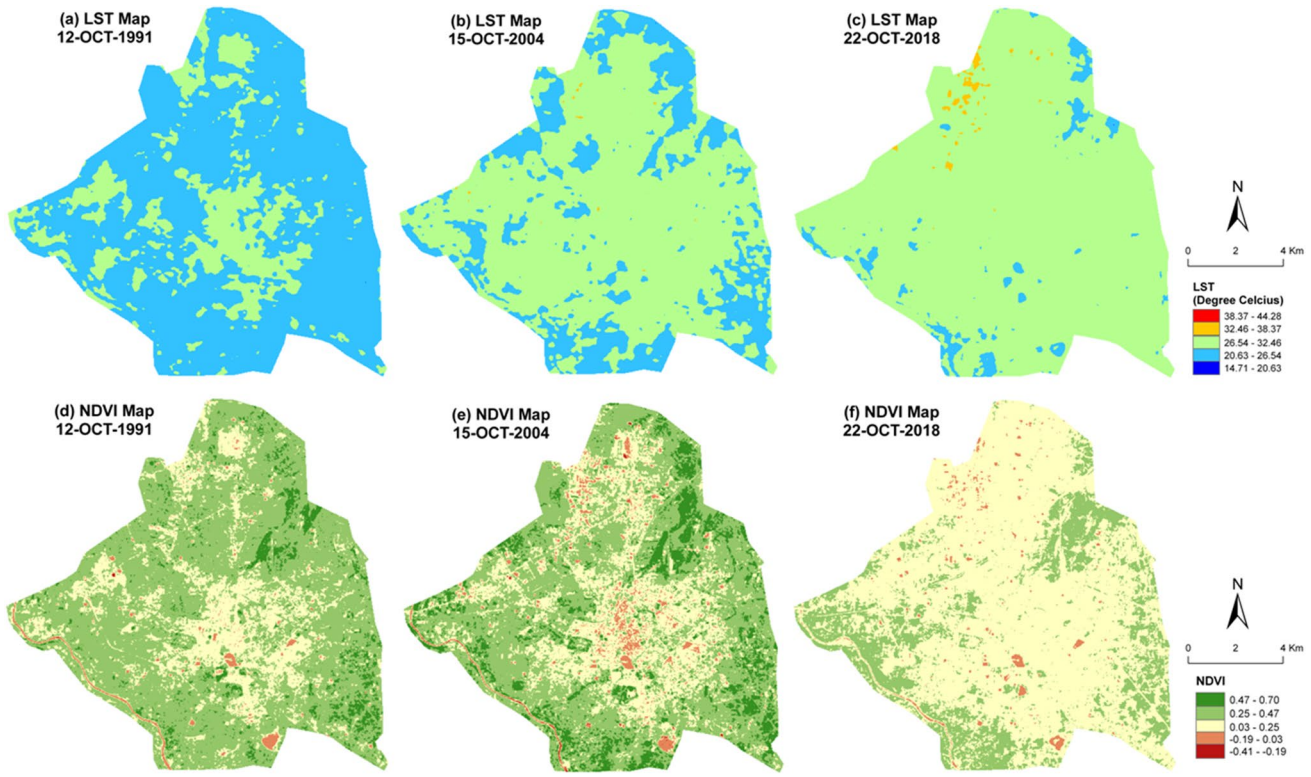

Fig. 5 Spatial distribution of LST in post-monsoon season: **a** 12-OCT-1991 **b** 15-OCT-2004 **c** 22-OCT-2018; spatial distribution of NDVI in post-monsoon season: **d** 12-OCT-1991 **e** 15-OCT-2004 **f** 22-OCT-2018

season, while it was negative in summer season. This relationship was also negative in Mashhad, Iran [57]. The relationship was strong negative in Berlin City for any season [95]. This correlation tends to be more negative with the increase of surface moisture [96–99]. The present study also found that the LST-NDVI correlation is negative, irrespective of any season. The value of correlation coefficient is inversely related to the surface moisture content, i.e., negativity of the relationship increases with the increase of surface moisture content.

5 Conclusion

The present study analyzes the spatial, temporal, and seasonal relationship of LST and NDVI in a tropical city of India using 12 Landsat data sets of four different seasons (winter, pre-monsoon, monsoon, and post-monsoon) for 1991, 2004, and 2018. The mono-window algorithm was applied in deriving LST. In general, the results showed that LST is inversely related to NDVI, irrespective of any season. In the post-monsoon season, the relationship was strong negative (− 0.63), while it was found weak negative (− 0.17) in winter. A moderate range of negativity (− 0.45) was noticed in pre-monsoon and monsoon season. The presence of healthy green plants and high moisture content in the air are the main responsible factors for high negativity. The LST-NDVI relationship varies for specific LULC types. The green area presents a strong negative (− 0.51) regression, while the built-up area and bare land presents a weak positive regression (0.14). The relationship is moderately positive (0.45) on water bodies. On vegetation, the LST-NDVI relationship was highly negative in the pre-monsoon (− 0.65), monsoon (− 0.52), and post-monsoon (− 0.58) seasons, while it was weak negative (− 0.28)

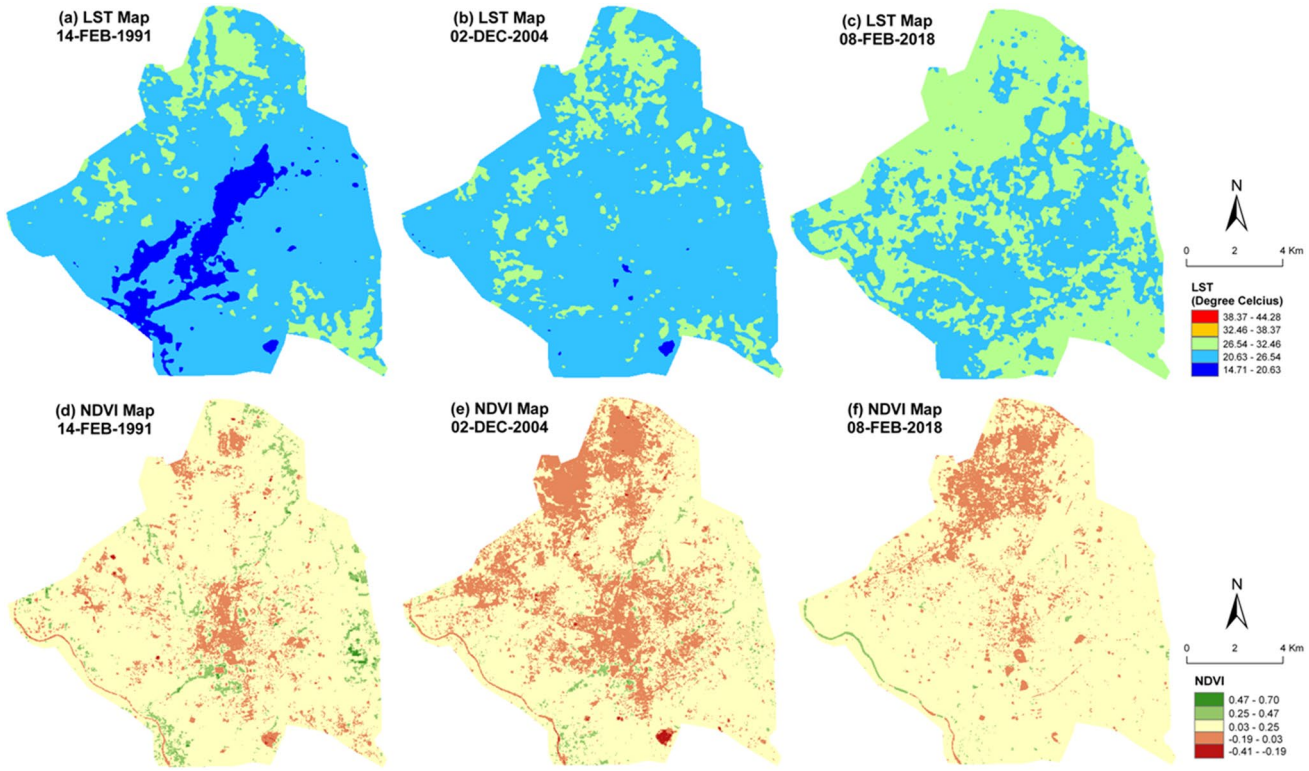

Fig. 6 Spatial distribution of LST in winter season: **a** 14-FEB-1991 **b** 02-DEC-2004 **c** 08-FEB-2018; spatial distribution of NDVI in winter season: **d** 14-FEB-1991 **e** 02-DEC-2004 **f** 08-FEB-2018

Table 4 Change in mean LST (°C) with the conversion of different types of LULC into the built-up area/bare land

Conversion of different LULC into built-up area/bare land	1991–2018			2004–2018		
	1991	2018	1991–2018	2004	2018	2004–2018
Vegetation	25.02	29.68	4.66	27.32	29.52	2.20
Water bodies	26.29	28.87	2.49	26.78	27.74	0.96
Built-up area/bare land	27.25	30.04	2.79	29.14	29.97	0.83
Total	25.51	29.74	4.23	28.25	29.74	1.49

in the winter season. The mean LST of the study area was increased by 5.16 °C during 1991–2018. The conversion of other lands into the built-up area and bare land influences a lot on the mean LST of the city. Both the changed and unchanged built-up area and bare land suffer from the increasing trend of LST. This result significantly presents the influence of climate change in Raipur City.

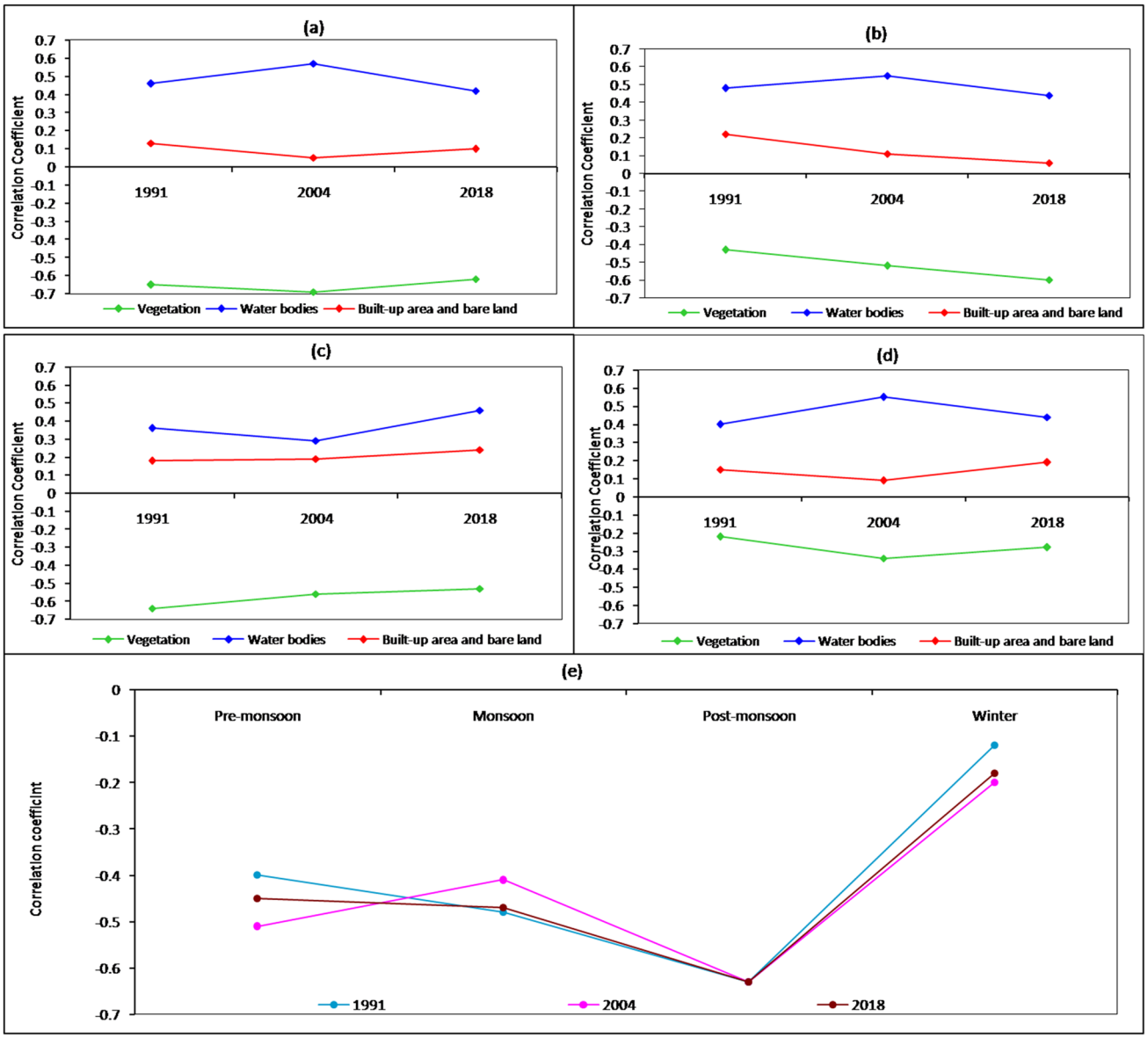

Fig. 7 Seasonal variation of LST-NDVI relationship on different types of LULC: **a** pre-monsoon **b** monsoon **c** post-monsoon **d** winter **e** overall

Acknowledgements The authors are indebted to the United States Geological Survey; India Meteorological Department; Meteorological Centre, Raipur; Regional Meteorological Centre, Nagpur; and Survey of India.

Compliance with ethical standards

Conflict of interest No potential conflict of interest was reported by the authors.

References

1. Foley JA, DeFries R, Asner GP, Barford C, Bonan G, Carpenter SR, Chapin FS, Coe MT, Daily GC, Gibbs HK et al (2005) Global consequences of land use. Science 309:570–574
2. Fu P, Weng Q (2016) A time series analysis of urbanization induced land use and land cover change and its impact on land surface temperature with landsat imagery. Remote Sens Environ 175:205–214
3. Grimm NB, Faeth SH, Golubiewski NE, Redman CL, Wu J, Bai X, Briggs JM, Grimm N (2008) Global change and the ecology of cities. Science 319:756–760
4. Liu H, Zhan Q, Yang C, Wang J (2018) Characterizing the spatio-temporal pattern of land surface temperature through time series clustering: based on the latent pattern and morphology. Remote Sens 10:654

5. Liu Y, Peng J, Wang Y (2018) Efficiency of landscape metrics characterizing urban land surface temperature. Landsc Urban Plan 180:36–53
6. Peng J, Ma J, Liu Q, Liu Y, Hu Y, Li Y, Yue Y (2018) Spatial-temporal change of land surface temperature across 285 cities in China: an urban-rural contrast perspective. Sci Total Environ 635:487–497
7. Patz JA, Campbell-Lendrum D, Holloway T, Foley JA (2005) Impact of regional climate change on human health. Nat Cell Boil 438:310–317
8. Huang S, Taniguchi M, Yamano M, Wang CH (2009) Detecting urbanization effects on surface and subsurface thermal environment—a case study of Osaka. Sci Total Environ 407:3142–3152
9. Zhou D, Xiao J, Bonafoni S, Berger C, Deilami K, Zhou Y, Frolking S, Yao R, Qiao Z, Sobrino JA (2019) Satellite remote sensing of surface urban heat islands: progress, challenges, and perspectives. Remote Sens 11:48
10. Guha S, Govil H, Dey A, Gill N (2020) A case study on the relationship between land surface temperature and land surface indices in Raipur City, India. Geogr Tidsskr. https://doi.org/10.1080/00167223.2020.1752272
11. Govil H, Guha S, Diwan P, Gill N, Dey A (2020) Analyzing linear relationships of LST with NDVI and MNDISI using various resolution levels of landsat 8 OLI and TIRS data. In: Sharma N, Chakrabarti A, Balas V (eds) Data management, analytics and innovation. Advances in intelligent systems and computing, vol 1042. Springer, Singapore, pp 171–184. https://doi.org/10.1007/978-981-32-9949-8_13
12. Guha S, Govil H (2020) An assessment on the relationship between land surface temperature and normalized difference vegetation index. Environ Dev Sustain. https://doi.org/10.1007/s10668-020-00657-6
13. Kalnay E, Cai M (2003) Impact of urbanization and land-use change on climate. Nat Cell Boil 423:528–531
14. Chen XL, Zhao HM, Li PX, Yi ZY (2006) Remote sensing image-based analysis of the relationship between urban heat island and land use/cover changes. Remote Sens Environ 104(2):133–146
15. Peng J, Jia J, Liu Y, Li H, Wu J (2018) Seasonal contrast of the dominant factors for spatial distribution of land surface temperature in urban areas. Remote Sens Environ 215:255–267
16. Berger C, Rosentreter J, Voltersen M, Baumgart C, Schmullius C, Hese S (2017) Spatio-temporal analysis of the relationship between 2D/3D urban site characteristics and land surface temperature. Remote Sens Environ 193:225–243
17. Du S, Xiong Z, Wang Y, Guo L (2016) Quantifying The Multilevel Effects Of Landscape Composition And Configuration On Land Surface Temperature. Remote Sens Environ 178:84–92
18. Peng J, Xie P, Liu Y, Ma J (2016) Urban thermal environment dynamics and associated landscape pattern factors: a case study in the beijing metropolitan region. Remote Sens Environ 173:145–155
19. He BJ, Zhao ZQ, Shen LD, Wang HB, Li LG, He BJ (2019) An approach to examining performances of cool/hot sources in mitigating/enhancing land surface temperature under different temperature backgrounds based on landsat 8 image. Sustain Cities Soc 44:416–427
20. Weng Q (2009) Thermal Infrared Remote Sensing for Urban Climate and Environmental Studies: methods, Applications, and Trends. ISPRS J Photogramm Sens 64:335–344
21. Fu P, Weng Q (2015) Temporal dynamics of land surface temperature from landsat TIR time series images. IEEE Geosci Sens Lett 12:1–5
22. Hao X, Li W, Deng H (2016) The oasis effect and summer temperature rise in arid regions-case study in Tarim Basin. Sci Rep 6:35418. https://doi.org/10.1038/srep35418
23. Tran DX, Pla F, Latorre-Carmona P, Myint SW, Caetano M, Kieu HV (2017) Characterizing the relationship between land use land cover change and land surface temperature. ISPRS J Photogramm Sens 124:119–132
24. Guha S, Govil H, Diwan P (2019) Analytical study of seasonal variability in land surface temperature with normalized difference vegetation index, normalized difference water index, normalized difference built-up index, and normalized multi-band drought index. J Appl Remote Sens 13(2):024518. https://doi.org/10.1117/1.JRS.13.024518
25. Hou GL, Zhang HY, Wang YQ, Qiao ZH, Zhang ZX (2010) Retrieval and spatial distribution of land surface temperature in the middle part of jilin province based on MODIS data. Sci Geogr Sin 30:421–427
26. Shigeto K (1994) Relation between vegetation, surface temperature, and surface composition in the Tokyo region during winter. Remote Sens Environ 50:52–60
27. Ghobadi Y, Pradhan B, Shafri HZM, Kabiri K (2014) Assessment of spatial relationship between land surface temperature and land use/cover retrieval from multi-temporal remote sensing data in South Karkheh Sub-basin, Iran. Arab J Geosci 8(1):525–537. https://doi.org/10.1007/s12517-013-1244-3
28. Stroppiana D, Antoninetti M, Brivio PA (2014) Seasonality of MODIS LST over Southern Italy and correlation with land cover, topography and solar radiation. Eur J Remote Sens 47:133–152
29. Li ZN et al (2016) Review of methods for land surface temperature derived from thermal infrared remotely sensed data. J Remote Sens 20:899–920
30. Estoque RC, Murayama Y, Myint SW (2017) Effects of landscape composition and pattern on land surface temperature: an urban heat island study in the megacities of Southeast Asia. Sci Total Environ 577:349–359
31. Wen LJ et al (2017) An analysis of land surface temperature (LST) and its influencing factors in summer in western Sichuan Plateau: a case study of Xichang City. Remote Sens Land Res 29:207–214
32. Zhao ZQ, He BJ, Li LG, Wang HB, Darko A (2017) Profile and concentric zonal analysis of relationships between land use/land cover and land surface temperature: case study of Shenyang, China. Energ Build 155:282–295. https://doi.org/10.1016/j.enbuild.2017.09.046
33. Ferrelli F, Huamantinco MA, Delgado DA, Piccolo MC (2018) Spatial and temporal analysis of the LST-NDVI relationship for the study of land cover changes and their contribution to urban planning in Monte Hermoso, Argentina. Doc Anal Geogr 64(1):25–47. https://doi.org/10.5565/rev/dag.355
34. Mahato S, Pal S (2018) Changing land surface temperature of a rural Rarh tract river basin of India. Remote Sens Appl Soc Environ 10:209–223. https://doi.org/10.1016/j.rsase.2018.04.005
35. Mathew A, Khandelwal S, Kaul N (2018) Spatio-temporal variations of surface temperatures of Ahmedabad city and its relationship with vegetation and urbanization parameters as indicators of surface temperatures. Remote Sens Appl Soc Environ 11:119–139. https://doi.org/10.1016/j.rsase.2018.05.003
36. Sannigrahi S et al (2018) Analyzing the role of biophysical compositions in minimizing urban land surface temperature and urban heating. Urban Climate. https://doi.org/10.1016/j.uclim.2017.10.002
37. Fatemi M, Narangifard M (2019) Monitoring LULC changes and its impact on the LST and NDVI in District 1 of Shiraz City. Arab J Geosci 12:127. https://doi.org/10.1007/s12517-019-4259-6

38. Filho WLFC, De Barros Santiago D, De Oliveira-Júnior JF, Da Silva Junior CA (2019) Impact of urban decadal advance on land use and land cover and surface temperature in the city of Maceió, Brazil. Land Use Policy 87:104026. https://doi.org/10.1016/j.landusepol.2019.104026
39. Mushore TD, Dube T, Manjowe M, Gumindogab W, Chemuira A, Rousta I, Obindi J, Mutanga O (2019) Remotely sensed retrieval of Local climate zones and their linkages to land surface temperature in Harare metropolitan city, Zimbabwe. Urban Clim 27:171–259. https://doi.org/10.1016/j.uclim.2018.12.006
40. Mushore TD, Odindi J, Dube T, Matongera TN, Mutanga O (2017) Remote sensing applications in monitoring urban growth impacts on in-and-out door thermal conditions: a review. Remote Sens Appl Soc Environ 8:83–93. https://doi.org/10.1016/j.rsase.2017.08.001
41. Mushore TD, Odindi J, Dube T, Mutanga O (2017) Prediction of future urban surface temperatures using medium resolution satellite data in Harare metropolitan city, Zimbabwe. Build Environ 122:397–410. https://doi.org/10.1016/j.buildenv.2017.06.033
42. Ullah S, Ahmad K, Sajjad RU, Abbasi AM, Nazeer A, Tahir AA (2019) Analysis and simulation of land cover changes and their impacts on land surface temperature in a lower Himalayan region. J Environ Manag 245:348–357. https://doi.org/10.1016/j.jenvman.2019.05.063
43. Nimish G, Bharath HA, Lalitha A (2020) Exploring temperature indices by deriving relationship between land surface temperature and urban landscape. Remote Sens Appl Soc Environ 18:100299. https://doi.org/10.1016/j.rsase.2020.100299
44. Sultana S, Satyanarayana ANV (2020) Assessment of urbanisation and urban heat island intensities using landsat imageries during 2000 – 2018 over a sub-tropical Indian City. Sustain Cities Soc 52:101846. https://doi.org/10.1016/j.scs.2019.101846
45. Smith RCG, Choudhury BJ (1990) On the correlation of indices of vegetation and surface temperature over south-eastern Australia. Int J Remote Sens 11:2113–2120
46. Hope AS, McDowell TP (1992) The relationship between surface temperature and a spectral vegetation index of a tall grass prairie: effects of burning and other landscape controls. Int J Remote Sens 13:2849–2863
47. Julien Y, Sobrino JA, Verhoef W (2006) Changes in land surface temperatures and NDVI values over Europe between 1982 and 1999. Remote Sens Environ 103:43–55
48. Yuan XL et al (2017) Vegetation changes and land surface feedbacks drive shifts in local temperatures over Central Asia. Sci Rep 7:3287. https://doi.org/10.1038/s41598017034322
49. Mondal A, Guha S, Mishra PK, Kundu S (2011) Land use/Land cover changes in Hugli Estuary using Fuzzy C-Mean algorithm. Int J Geomat Geosci 2(2): 613–626
50. Carlson TN, Ripley DA (1997) On the relation between NDVI, fractional vegetation cover, and leaf area index. Remote Sens Environ 62:241–252. https://doi.org/10.1016/S0034-4257(97)00104-1
51. Sobrino JA, Jimenez-Munoz JC, Paolini L (2004) Land surface temperature retrieval from Landsat TM5. Remote Sens Environ 9:434–440. https://doi.org/10.1016/j.rse.2004.02.003
52. Gutman G, Ignatov A (1998) The derivation of the green vegetation fraction from NOAA/AVHRR data for use in numerical weather prediction models. Int J Remote Sens 19(8):1533–1543. https://doi.org/10.1080/014311698215333
53. Goward SN, Xue YK, Czajkowski KP (2002) Evaluating land surface moisture conditions from the remotely sensed temperature/vegetation index measurements: an exploration with the simplified simple biosphere model. Remote Sens Environ 79:225–242. https://doi.org/10.1016/S0034-4257(01)00275-9
54. Voogt JA, Oke TR (2003) Thermal remote sensing of urban climates. Remote Sens Environ 86:370–384. https://doi.org/10.1016/S0034-4257(03)00079-8
55. Weng QH, Lu DS, Schubring J (2004) Estimation of land surface temperature-vegetation abundance relationship for urban heat island studies. Remote Sens Environ 89:467–483. https://doi.org/10.1016/j.rse.2003.11.005
56. Yue W, Xu J, Tan W, Xu L (2007) The relationship between land surface temperature and NDVI with remote sensing. Application to Shanghai Landsat 7 ETM + data. Int J Remote Sens 28:3205–3226. https://doi.org/10.1080/01431160500306906
57. Gorgani SA, Panahi M, Rezaie F (2013) The relationship between NDVI and LST in the Urban area of Mashhad, Iran. In: International conference on civil engineering architecture and urban sustainable development. November, Tabriz, Iran
58. Govil H, Guha S, Dey A, Gill N (2019) Seasonal evaluation of downscaled land surface temperature: a case study in a humid tropical city. Heliyon 5(6):e01923. https://doi.org/10.1016/j.heliyon.2019.e01923
59. Cui L, Wang L, Qu S, Singh RP, Lai Z, Jiang L, Yao R (2019) Association analysis between spatiotemporal variation of vegetation greenness and precipitation/temperature in the Yangtze River Basin (China). Environ Sci Pollut Res 25(22):21867–21878. https://doi.org/10.1007/s11356-018-2340-4
60. Cui L, Wang L, Qu S, Singh RP, Lai Z, Yao R (2019) Spatiotemporal extremes of temperature and precipitation during 1960–2015 in the Yangtze River Basin (China) and impacts on vegetation dynamics. Theor Appl Climatol 136(1–2):675–692. https://doi.org/10.1007/s00704-018-2519-0
61. Gui X, Wang L, Yao R, Yu D, Li C (2019) Investigating the urbanization process and its impact on vegetation change and urban heat island in Wuhan, China. Environ Sci Pollut Res 26(30):30808–30825. https://doi.org/10.1007/s11356-019-06273-w
62. Qu S, Wang L, Lin A, Yu D, Yuan M, Li C (2020) What drives the vegetation restoration in Yangtze River basin, China: climate change or anthropogenic factors? Ecol Indic 108:105724. https://doi.org/10.1016/j.ecolind.2019.105724
63. Qu S, Wang L, Lin A, Zhu H, Yuan M (2018) What drives the vegetation restoration in Yangtze River basin, China: climate change or anthropogenic factors? Ecol Indic 90:438–450. https://doi.org/10.1016/j.ecolind.2018.03.029
64. Yao R, Cao J, Wang L, Zhang W, Wu X (2019) Urbanization effects on vegetation cover in major African cities during 2001–2017. Int J Appl Earth Obs 75:44–53. https://doi.org/10.1016/j.jag.2018.10.011
65. Yao R, Wang L, Huang X, Chen J, Li J, Niu Z (2018) Less sensitive of urban surface to climate variability than rural in Northern China. Sci Total Environ 628–629:650–660. https://doi.org/10.1016/j.scitotenv.2018.02.087
66. Yao R, Wang L, Huang X, Niu Z, Liu F, Wang Q (2017) Temporal trends of surface urban heat islands and associated determinants in major Chinese cities. Sci Total Environ 609:742–754. https://doi.org/10.1016/j.scitotenv.2017.07.217
67. Yuan M, Wang L, Lin A, Liu Z, Qu S (2020) Vegetation green up under the influence of daily minimum temperature and urbanization in the Yellow River Basin, China. Ecol Indic 108:105760. https://doi.org/10.1016/j.ecolind.2019.105760
68. Kumar D, Shekhar S (2015) Statistical analysis of land surface temperature-vegetation indexes relationship through thermal remote sensing. Ecotox Environ Safe 121:39–44. https://doi.org/10.1016/j.ecoenv.2015.07.004
69. Kikon N, Singh P, Singh SK, Vyas A (2016) Assessment of urban heat islands (UHI) of Noida City, India using multi-temporal satellite data. Sustain Cities Soc 22:19–28. https://doi.org/10.1016/j.scs.2016.01.005

70. Singh P, Kikon N, Verma P (2017) Impact of land use change and urbanization on urban heat island in Lucknow city, Central India. A remote sensing based estimate. Sustain Cities Soc 32:100–114. https://doi.org/10.1016/j.scs.2017.02.018
71. Mathew A, Khandelwal S, Kaul N (2017) Investigating spatial and seasonal variations of urban heat island effect over Jaipur city and its relationship with vegetation, urbanization and elevation parameters. Sustain Cities Soc 35:157–177. https://doi.org/10.1016/j.scs.2017.07.013
72. Guha S, Govil H, Gill N, Dey A (2020) Analytical study on the relationship between land surface temperature and land use/land cover indices. Ann GIS 26(2):201–216. https://doi.org/10.1080/19475683.2020.1754291
73. https://www.earthexplorer.usgs.gov
74. http://www.surveyofindia.gov.in
75. https://www.mausam.imd.gov.in
76. Qin Z, Karnieli A, Barliner P (2001) A mono-window algorithm for retrieving land surface temperature from landsat TM data and its application to the Israel–Egypt border region. Int J Remote Sens 22(18):3719–3746. https://doi.org/10.1080/01431160010006971
77. Wang F, Qin Z, Song C, Tu L, Karnieli A, Zhao S (2015) An improved mono-window algorithm for land surface temperature retrieval from Landsat 8 thermal infrared sensor data. Remote Sens 7(4):4268–4289
78. Wang L, Lu Y, Yao Y (2019) Comparison of three algorithms for the retrieval of land surface temperature from Landsat 8 images. Sensors 19(22):5049
79. Sekertekin A, Bonafoni S (2020) Land surface temperature retrieval from landsat 5, 7, and 8 over rural areas: assessment of different retrieval algorithms and emissivity models and toolbox implementation. Remote Sens 12(2):294
80. Zanter K (2019) Landsat 8 (L8) Data users handbook; EROS: Sioux Falls, SD, USA
81. Wukelic GE, Gibbons DE, Martucci LM, Foote HP (1989) Radiometric calibration of landsat thematic mapper thermal band. Remote Sens Environ 28:339–347
82. Sobrino JA, Raissouni N, Li Z (2001) A comparative study of land surface emissivity retrieval from NOAA data. Remote Sens Environ 75(2):256–266
83. Yang J, Qiu J (1996) The empirical expressions of the relation between precipitable water and ground water vapor pressure for some areas in China. Sci Atmos Sinica 20:620–626
84. http://www.imdraipur.gov.in
85. http://www.imdnagpur.gov.in
86. Sun Q, Tan J, Xu Y (2010) An ERDAS image processing method for retrieving LST and describing urban heat evolution: a case study in the Pearl River Delta Region in South China. Environ Earth Sci 59:1047–1055
87. Tucker CJ (1979) Red and photographic infrared linear combinations for monitoring vegetation. Remote Sens Environ 8(2):127–150
88. Purevdorj TS, Tateishi R, Ishiyama T, Honda Y (1998) Relationships between percent vegetation cover and vegetation indices. Int J Remote Sens 19:3519–3535
89. Ke YH, Im J, Lee J, Gong HL, Ryu Y (2015) Characteristics of landsat 8 oli-derived NDVI by comparison with multiple satellite sensors and in-situ observations. Remote Sens Environ 164:298–313. https://doi.org/10.1016/j.rse.2015.04.004
90. Nigatu W, Dick ØB, Tveite H (2014) GIS based mapping of land cover changes utilizing multi-temporal remotely sensed image data in lake Hawassa watershed. Ethiopia. Environ Monit Assess 186(3):1765–1780. https://doi.org/10.1007/s10661-013-3491-x
91. https://www.esri.com
92. Liang BP, Li Y, Chen KZ (2012) A research on land features and correlation between NDVI and land surface temperature in Guilin City. Remote Sens Tech Appl 27:429–435
93. Cao L, Hu HW, Meng XL, Li JX (2011) Relationships between land surface temperature and key landscape elements in urban area. Chin J Ecol 30:2329–2334
94. Sun D, Kafatos M (2007) Note on the NDVI-LST relationship and the use of temperature-related drought indices over North America. Geophys Res Lett. https://doi.org/10.1029/2007GL031485
95. Marzban F, Sodoudi S, Preusker R (2018) The influence of land-cover type on the relationship between LST-NDVI and LST-T_{air}. Int J Remote Sens 39(5):1377–1398. https://doi.org/10.1080/01431161.2017.1462386
96. Lambin EF, Ehrlich D (1996) The surface tenperature-vegetation index space for land use and land cover change analysis. Int J Remote Sens 17:463–487. https://doi.org/10.1080/01431169608949021
97. Moran MS, Clarke TR, Inouie Y, Vidal A (1994) Estianting crop water-deficit using the relation between surface air-temperature and spectral vegetation index. Remote Sens Environ 49:246–263. https://doi.org/10.1016/0034-4257(94)90020-5
98. Sandholt I, Rasmussen K, Andersen J (2002) A simple interpretation of the surface temperature/vegetation index space for assessment of surface moisture status. Remote Sens Environ 79:213–224. https://doi.org/10.1016/s0034-4257(01)00274-7
99. Prehodko L, Goward SN (1997) Estimation of air temperature from remotely sensed surface observations. Remote Sens Environ 60:335–346. https://doi.org/10.1016/S0034-4257(96)00216-7
100. Coll C et al (2010) Validation of Landsat-7/ETM + thermal-band calibration and atmospheric correction with ground-based measurements. IEEE Trans Geosci Remote Sens 48(1):547–555
101. Guha S, Govil H, Mukherjee S (2017) Dynamic analysis and ecological evaluation of urban heat islands in Raipur city, India. J Appl Remote Sens 11(3):036020. https://doi.org/10.1117/1.JRS.11.036020
102. Guha S, Govil H, Diwan P (2020) Monitoring LST-NDVI Relationship Using Premonsoon Landsat Datasets. Adv Meteorol 2020:4539684. https://doi.org/10.1155/2020/4539684
103. Guha S, Govil H, Dey A, Gill N (2018) Analytical study of land surface temperature with NDVI and NDBI using Landsat 8 OLI/TIRS data in Florence and Naples city, Italy. Eur J Remote Sens 51(1):667–678. https://doi.org/10.1080/22797254.2018.1474494
104. Guha S, Govil H (2020) Seasonal impact on the relationship between land surface temperature and normalized difference vegetation index in an urban landscape. Geocarto Int. https://doi.org/ 10.1080/10106049.2020.1815867

Publisher's Note Springer Nature remains neutral with regard to jurisdictional claims in published maps and institutional affiliations.